ISSN 1995-0780, Nanotechnologies in Russia, 2019, Vol. 14, Nos. 11–12, pp. 607–612. © Pleiades Publishing, Ltd., 2019.

NANOBIOMEDICINE AND NANOPHARMACEUTICALS

Facile Synthesis of Ultrasmall, Highly Stable, and Biocompatible Gold Nanoparticles Stabilized with Lipoic Acid: Cytotoxicity and Structural Characterization

Delfino Cornejo-Monroy[a], Betania Sánchez-Santamaria[a], Erwin Adán Martínez-Gómez[a], Imelda Olivas-Armendáriz[a], Alfredo Villanueva-Montellano[a], José Saúl Arias-Cerón[b], and Victor M. Castaño[c,*]

[a] *Universidad Autónoma de Ciudad Juárez, Colonia Partido Romero, Juárez, Chihuahua, C.P. 32310 México*

[b] *Centro de Investigación y de Estudios Avanzados del I.P.N., San Pedro Zacatenco, Ciudad de México, C.P. 07360 México*

[c] *Universidad Nacional Autónoma de México, Querétaro, Querétaro, C.P. 76230 México*

*****e-mail: victor.m.castano@gmail.com*

Received February 21, 2020; revised February 21, 2020; accepted March 25, 2020

Abstract—Using the colloidal method, and lipoic acid as a stabilizer, ultrasmall gold nanoparticles with an average size of 2.5 nm were synthesized. They are highly stable, have COOH functional groups, at concentrations lower than 100 μg/mL are non-cytotoxic, and the synthesis route is simple and economical. UV–Vis, FT-IR, Raman, and TEM spectroscopy were used to analyze their stability, composition and morphology. Furthermore, the cytotoxicity of the gold nanoparticles was evaluated by MTT assay.

DOI: 10.1134/S199507801906003X

1. INTRODUCTION

Nanogold is probably one of the most fascinating materials in the nanoscience and nanotechnology fields due to its physical and chemical properties [1, 2]. More specifically, due to its relatively simple synthesis, resistance to corrosion, biocompatibility, and uncomplicated functionalization, as well as conjugation with a great variety of chemical and biological entities [3]. Gold nanostructures have shown to have potential applications in many research areas. In medicine [4], ultrasmall nanoparticles below 5 nm have unique advantages in the human body due to their relatively rapid elimination, good uptake, and favorable interaction with radiation [2, 5]. For instance, gold nanostructures have been proven as effective sensors [6], chemical carriers [7, 8], and more recently as theranostic agents [4, 9, 10]. To be successful in any application, stability of nanogold has to be strong enough to resist aggressive conditions, such as laser irradiance, acid and basic mediums, salty medium, powder form, as well as biological conditions [11, 12]. Many chemical or biological entities have been used to give good stability to gold nanostructures, such as polyvinylpyrrolidone (PVP), polyethylene glycol (PEG), xanthan gum, acacia gum, oleylamine and others [13–18]. In addition to the high stability, it is desired that the entity used to produce stability, also create functional groups. The functional groups are very useful tools to attach biological entities which give additional extraordinary physical and chemical properties that are necessary to achieve specific requirements for a determined application [19]. However, many entities used to stabilize do not create remarkable functional groups, and the processes generally require many steps, hazardous chemicals and they are time consuming [20–22]; all these entail expensive gold nanoparticles [2]. Furthemore, in biomedical applications, the interactions between surface funtionalized nanoparticles and cells can damage the integrity of the membrane structure [23], affecting viability or cellular functions [24, 25]. In this paper, a simple and economical method is presented to stabilize ultrasmall gold nanoparticles using lipoic acid. In medicine lipoic acid (LA) is used to treat many diseases, due to its antioxidant properties [26]. Our gold nanoparticles stabilized with lipoic acid (GNPs@LA) are very stable under different conditions, and have COOH functional groups on the nanoparticle's surface which can be used to conjugate biological entities for specific applications. UV–Vis, FT-IR, Raman spectroscopies, and TEM were used to analyze their stability, composition and morphology. Moreover, the cytotoxicity of GNPs@LA at different concentrations was tested at different concentrations giving favorable results.

2. EXPERIMENTAL DETAILS

2.1. Materials

GNPs@LA were synthesized using: gold chloride 1% solution (Salt Lake Metals), sodium borohydride powder ≥98% (Sigma-Aldrich), (±)-α-lipoic acid minimum 99% titration (Sigma), ethyl alcohol 96% G.L (AZ), and ultrapure water >18 MΩ cm. To promote the agglomeration sodium chloride NaCl 99.8% (Bioland Scientific LLC), and PBS 1.X were used. For the cytotoxicity test the materials used were: hematoxylin (Sigma-Aldrich), eosine 99% (Sigma-Aldrich), PBS 1.X, glutaraldehyde GradeII 25% in H_2O (Sigma-Aldrich) and dimethyl sulfoxide DMSO ≥ 99.9% (Sigma-Aldrich).

2.2. Equipment

Laboratory stirrer PC 410 (Corning®), analytical balance (Ohaus®), water purification system (Water-Pro PS, Labconco®), rotary evaporator with vacuum pump and controller (Buchi R-3 Rotavapor), UV/Vis spectrophotometer 190–1100 ± 1 nm (Zhejiang Holdwell Group), infrared spectrometer (M 530, Buck Scientific), Raman spectrometer (Horiba Jobin HR 800), transmission electron microscope (JEOL JEM-ARM200F), fluorescence microscope 100× (Zeiss N-Achroplan) and microplate spectrophotometer (Benchmark Plus) and digital camera SLR D800 (Nikon®).

2.3. Preparation of Bare Gold Nanoparticles and Gold Nanoparticles Stabilized with Lipoic Acid

Based on the "bottom-up" methodology and specifically in the colloidal method, gold nanoparticles with an average size of 2.5 nm were synthesized and stabilized using gold chloride as a precursor, sodium borohydride as a reducer and lipoic acid as a stabilizer. To prepare 700 mL of aqueous colloidal solution, 6.3 mL of gold chloride solution was added to an Erlenmeyer flask contaning water at 10°C and under vigorous agitation; once the solution was mixed, 85 mg of sodium borohydride mixed in 7 mL of water were added. Up to this step, bare gold nanoparticles were synthesized. Approximately, 30 s after the addition of sodium borohydride, 100 mg of lipoic acid mixed in a solution of 7 mL of ethanol-water (1 : 1 vol./vol.) was added to the colloid to obtain gold nanoparticles stabilized with lipoic acid (GNPs@LA).

2.4. Cytotoxicity Assay

The cytotoxicity of the GNPs@LA was analyzed through the metabolic reduction of the fibroblasts to the MTT reagent, converting it to formazan. To perform this test, concentrations of: 20, 40, 60, 80, 100, 250, 500, 750, and 1000 μg/mL of GNPs@LA were placed in a 24-well plate, as well as a control, which were seeded and incubated with 20000 mouse fibroblast cells in D-MEM supplemented with fetal bovine serum (FBS) and penicillin–streptomycin. After 24 h, the incubation medium was removed and 200 μL of D-MEM solution, containing 10% FBS, 1% antibiotic, and 50 μL of MTT (5 mg/mL in PBS) were added. Then, it was incubated at 37°C for 2 h. The resulting formazan product was dissolved in dimethyl sulfoxide and the absorbance at 570 nm was measured using a Benchmark Plus, micro-plate spectrophotometer. Positive controls were also prepared for comparison purposes. Statistical significant was determined by Student's *t*-test. Significant was described at $p < 0.05$. The GNPs@LA cultured with fibroblasts were stained with hematoxylin and eosin for cell morphology examination.

2.5. Tests to Analyze the Stability of the Gold Nanoparticles

To test the stability of bare and stabilized gold nanoparticles, three different agglomeration promoters were used: NaCl, PBS, and evaporation of the water. NaCl was added to the colloid to a concentration of 10 wt %, PBS to 50 vol %, and water of the colloid was removed up to obtain powder.

3. RESULTS AND DISCUSSION

3.1. Photographs of the Colloidal Solutions

As we can be seen in Fig. 1 GNPs show a characteristic red-orange color, in contrast, GNPs@LA exhibit a magenta color. Regarding the stability, it is observed that GNPs are rapidly destabilized with the addition of NaCl, PBS, or both, being appreciable due to the change of color from red-orange to blue-gray when compared with those stabilized with LA where it can be seen that there are no significant changes in the color of the colloids.

3.2. UV–Vis Spectroscopy

GNPs show a characteristic peak around 496 nm (Fig. 2a). Using the model proposed by Haiss et al. [27], the estimated particle size from UV–Vis spectra is lower than 3 nm. After the addition of LA the corresponding peak moves to higher wavelengths (Fig. 2b), GNPs@LA have a characteristic peak around 498 nm which is an indicative that the lipoic acid was absorbed on the gold nanoparticles surface. To analyze the stability of colloids, NaCl and PBS was used to promote agglomeration; comparing GNPs + NaCl, GNPs + PBS, GNPs + NaCl + PBS spectra versus GNPs spectrum there is a very significant difference, NaCl and PBS destabilized almost instantly bare gold nanoparticles, but there is no difference between the GNPs@LA spectrum with GNPs@LA + NaCl, GNPs@LA + PBS, and GNPs@LA + NaCl + PBS spectra, which is an indicative that LA stabilizes gold

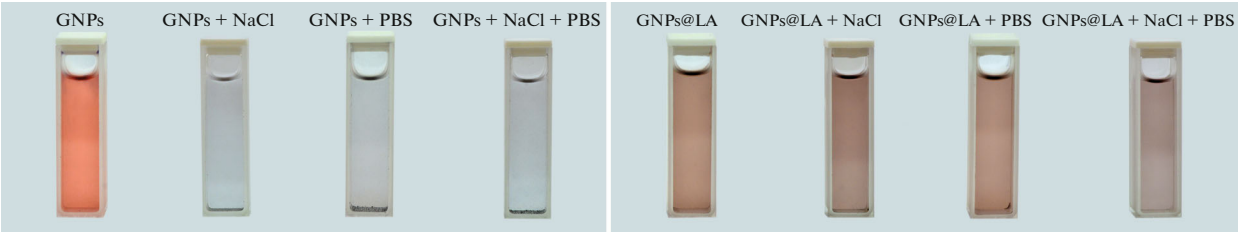

Fig. 1. (Color online) Photographs of the colloidal solutions.

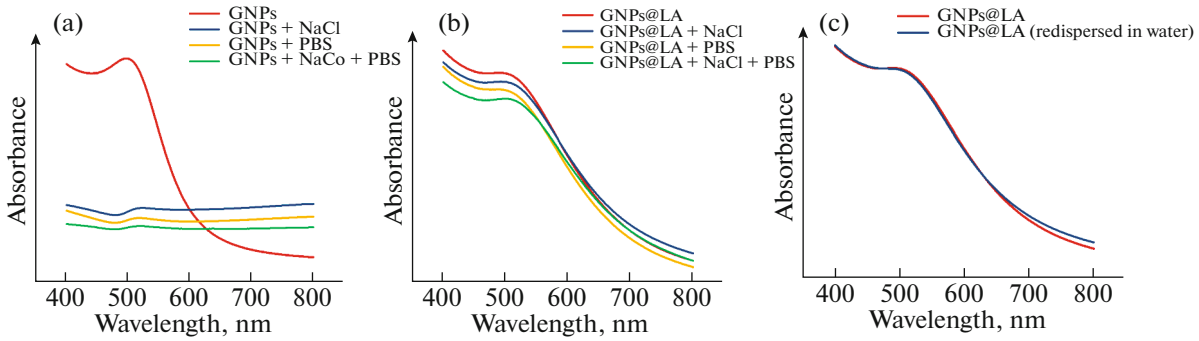

Fig. 2. (Color online) UV–Vis spectra of coloidal gold nanoparticles, (a) GNPs and GNPs with agglomeration promoters, (b) GNPs@LA and GNPs@LA with agglomeration promoters, and (c) GNPs@LA versus GNPs@LA redispersed in water after dried.

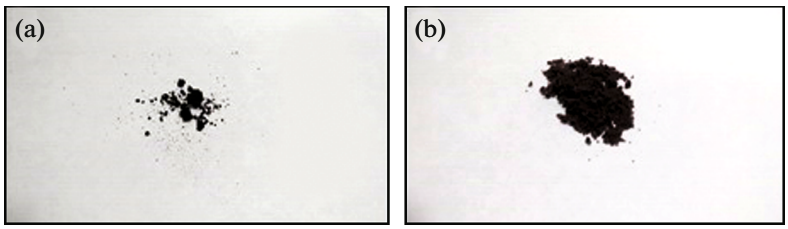

Fig. 3. (Color online) Photographs of (a) GNPs@LA and (b) GNPs@LA + NaCl both in powder form.

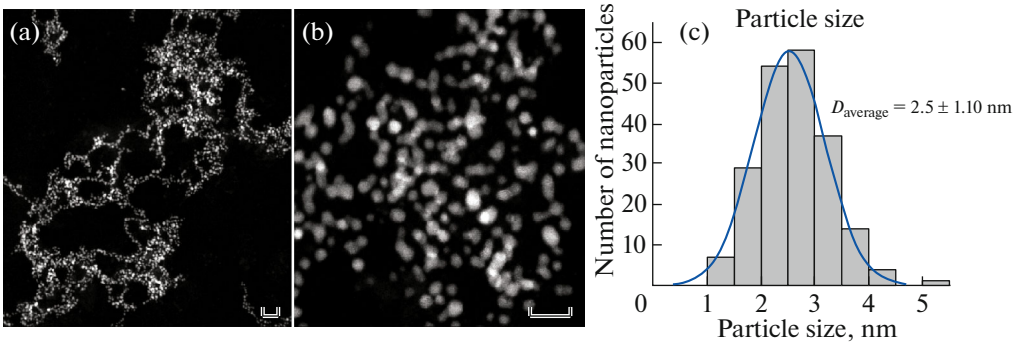

Fig. 4. (Color online) TEM micrographs of GNPs@LA at different magnifications. Scale bars (a) 20 nm, (b) 10 nm, and (c) size distribution histogram.

nanoparticles and prevents agglomeration. Additionally, as we can see in the UV–Vis results, powder of GNPs@LA can be easily redispersed in water without relevant effect on nanoparticles properties, where it is observed that the peak remains in the same position (Fig. 2c).

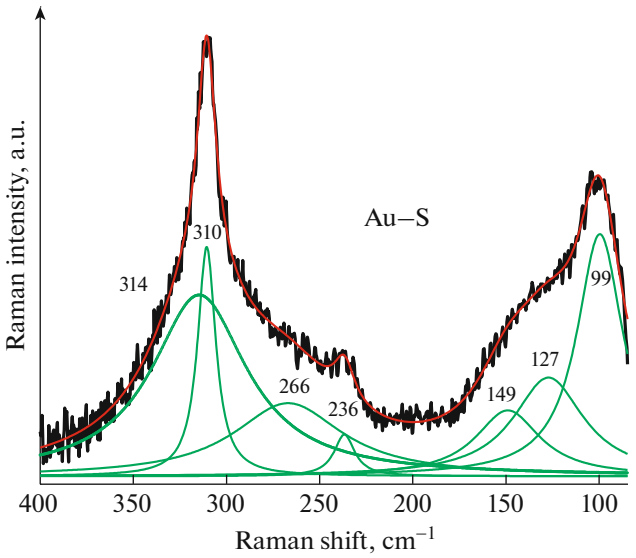

Fig. 5. (Color online) Raman spectra of GNPs@LA.

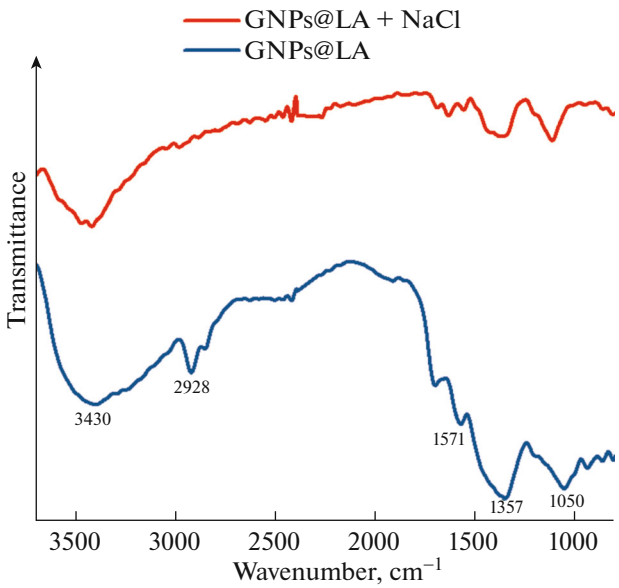

Fig. 6. (Color online) FTIR spectrum of GNPs@LA and GNPs@LA + NaCl.

3.3. Powder of GNPs@LA

Powder of GNPs@LA and GNPs@LA + NaCl was obtained using the rotary evaporator. Powders showed a dark brown color. GNPs@LA powder was like a sticky paste and darker (Fig. 3a), in contrast GNPs@LA + NaCl powder was easier to handle, like a powder (Fig. 3b). Both powders were redispersed in water without any effort, and without perceptive effect on their properties.

3.4. Transmission Electron Microscopy

The morphology and dispersion of GNPs@LA were visualized using TEM. Figure 4 clearly indicates that GNPs@LA were well dispersed, with almost spherical shape, not agglomerated, and an average size of 2.5 ± 1.10 nm. These sizes correspond to the UV–Vis spectra.

3.5. Raman Spectroscopy

GNPs@LA were analyzed using Raman scattering (532 nm). The single Raman spectra was used to identify the synthesis of the GNPs. These spectra was taken several times and we used long integration times in order to reduce noise (discard false peaks) and identify real vibrations. Figure 5 shows two asymmetric fundamental Raman bands around 400 and 100 cm^{-1}, which can be deconvoluted in seven Loretzian line shape signals as shown in Fig. 5, which are observed at 314, 310, 266, 236, 149, 127, and 99 cm^{-1}. Mainly associated with Au–S stretching and breathing modes due to the different nature of the Au–S bonds involved. Au–S modes have been assigned both experimentally and theoretically by Varnholt et al. [28].

3.6. Infrared Spectroscopy

The FTIR spectrum of GNPs@LA is show in Fig. 6. We compared GNPs@LA and GNPs@LA + NaCl spectrum and it is found that the principal absorptions bands are present in both samples which is an indicative of the high stability of the gold nanoparticles. FTIR spectrum shows six principal absoptions bands at 3430, 2928, 1571, 1357, 1115, and 1050 cm^{-1}. The bands present at 3430 and about 2928 cm^{-1} in the

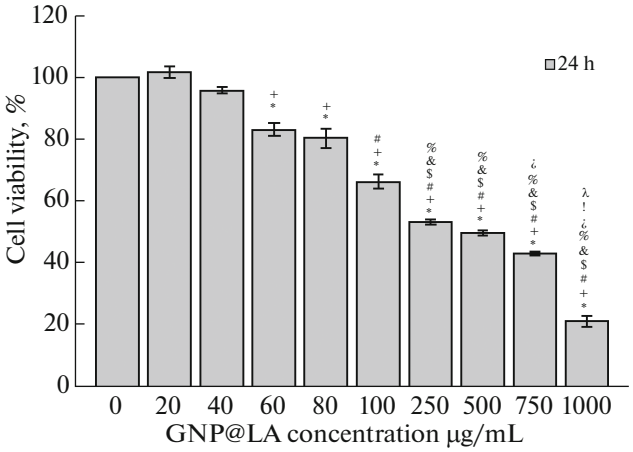

Fig. 7. Effects of GNPs on cellular viability.*: significant difference compared to control; +: significant difference compared to 20; #: significant difference compared to 40, $: significant difference compared to 60, &: significant difference compared to 80, %: significant difference compared to 100, ¿: significant difference compared to 250, !: significant difference compared to 500, λ: significant difference compared to 750 (p = 0.05, comparison is made between samples of the same day).

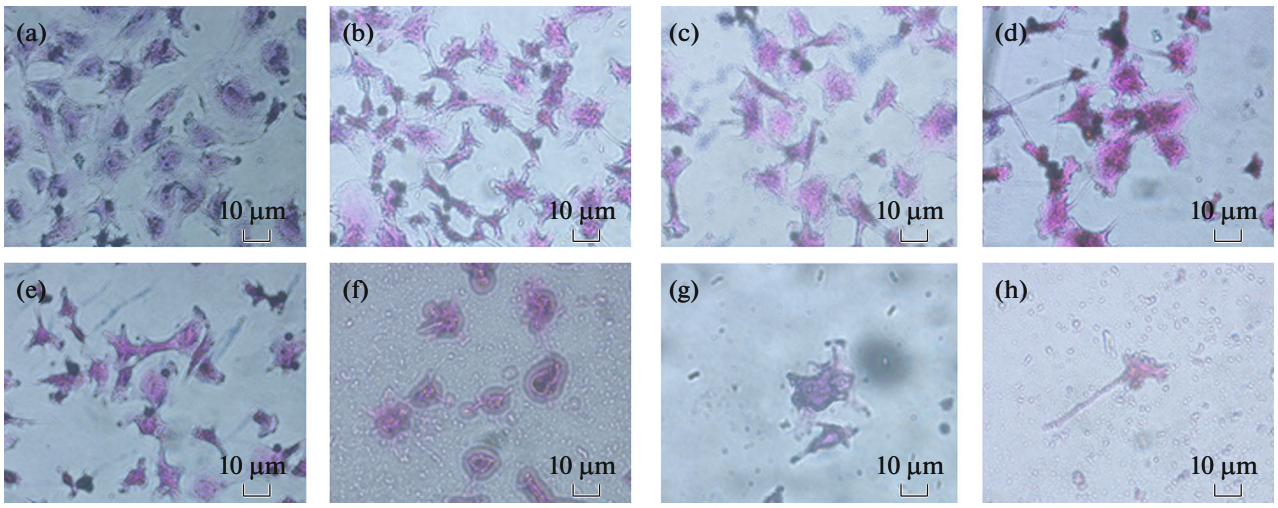

Fig. 8. (Color online) Fibroblast morphology at different concentrations after 24 h: (a) control, (b) 20, (c) 60, (d) 100, (e) 250, (f) 500, (g) 750, and (h) 1000 μg/mL.

spectrum can be attributed to the presence of water on the surface of nanoparticles and C–H bonds present in long chain hydrocarbon, respectively [29, 30]. The peak appearing at 1571 cm^{-1} corresponds to carbonyl group [31]. The peak corresponding to the functional group COOH was perceived at 1357 cm^{-1} [29]. The peaks observed at 1115 and 1050 cm^{-1} were not identified.

3.7. Cytotoxicity Assay

The effect of GNPs@LA on cell viability was evaluated by MTT assay (Fig. 7). It can be observed through mitochondrial activity that concentrations lower than 100 μg/mL do not present toxic effects at the cellular level, allowing us to verify that there were no cellular metabolism affectations after the exposure to the nanoparticles. On the other hand at higher concentrations of GNPs@LA there is a reduction in the number of viable cells showing a damage in mitochondrial activity, presenting a toxic effect according to ISO 10993-5 [32].

Figure 8 shows images of the fibroblasts, of the different concentrations of GNPs@LA, at 24 h of culture. More cells were observed in the control and concentrations lower than 100 μg/mL, coinciding with the MTT assay results. Cells of spheroidal (nodular) morphology and flattened cells that, according to Misra et al. are due to cell division [33]. In addition, cytoplasmic prolongations and extracellular matrix secreted by the cells are perceived. On the other hand, in the images of concentrations of nanoparticles greater than 100 μg/mL, fewer cells are observed, with changes in cellular morphology and cell membrane damage very evident at 500 μg/mL. The previous results show a relationship between the percentage of cellular viability and concentration of nanoparticles.

4. CONCLUSIONS

Ultrasmall GNPs stabilized with LA evaluated by MMT assay dot not present toxic effects at a cellular level at concentrations lower than 100 μg/mL. LA is attached to GNPs through Au–S bonds, prevents the agglomeration and creates COOH groups. These characteristics are useful for industrial and biomedical applications. TEM results exhibited that GNPs are well dispersed, with almost spherical shape, not agglomerated, and an average size of 2.5 nm. UV–Vis, FTIR, and Raman spectroscopy confirm that LA is acting as a capping agent. Finally, we claim that our proposed route of GNPs synthesis is simple, economical, and does not require expensive equipment.

ACKNOWLEDGMENTS

The authors are indebted to Dr. M. Pérez-González, S.A. Tomás, and Dr. Genoveva Hernández-Padrón for their technical support.

REFERENCES

1. L. Tamayo, H. Palza, J. Bejarano, and P. Zapata, "Polymer composites with metal nanoparticles: Synthesis, properties, and application polymer composites with functionalized nanoparticles," in *Polymer Composites with Functionalized Nanoparticles* (Elsevier, Amsterdam, 2019), pp. 249–286.
2. K. Haume et al., "Gold nanoparticles for cancer radiotherapy: A review," Cancer Nanotechnol. **7**, 8 (2016).
3. R. Herizchi, E. Abbasi, M. Milani, and A. Akbarzadeh, "Current methods for synthesis of gold nanoparticles," Artif. Cells, Nanomed. Biotechnol. **44**, 596–602 (2016).
4. J. Guo, K. Rahme, Y. He, L. Li, J. Holmes, and C. O'Driscoll, "Gold nanoparticles enlighten the fu-

ture of cancer theranostics," Int. J. Nanomed. **12**, 6131–6152 (2017).

5. K. Huang et al., "Size-dependent localization and penetration of ultrasmall gold nanoparticles in cancer cells, multicellular spheroids, and tumors in vivo," ACS Nano **6**, 4483–4493 (2012).
6. S. Afonso et al., "Electrochemical detection of Salmonella using gold nanoparticles," Biosens. Bioelectron. **40**, 121–126 (2013).
7. S. Parveen, R. Misra, and S. Sahoo, "Nanoparticles: A boon to drug delivery, therapeutics, diagnostics, and imaging," Nanomed. Nanotechnol., Biol. Med. **8**, 147–166 (2012).
8. H. Daraee, A. Eatemadi, E. Abbasi, S. Aval, M. Kouhi, and A. Akbarzadeh, "Application of gold nanoparticles in biomedical and drug delivery," Artif. Cells, Nanomed. Biotechnol. **44**, 410–422 (2014).
9. S. Patra, S. Mukherjee, A. Barui, A. Ganguly, B. Sreedhar, and C. Patra, "Green synthesis, characterization of gold and silver nanoparticles and their potential application for cancer therapeutics," Mater. Sci. Eng. C **53**, 298–309 (2015).
10. P. Kesharwani, H. Choudhury, J. Meher, M. Pandey, and B. Gorain, "Dendrimer-entrapped gold nanoparticles as promising nanocarriers for anticancer therapeutics and imaging," Prog. Mater. Sci. **103**, 484–508 (2019).
11. D. Cassano et al., "Biodegradable ultrasmall-in-nano gold architectures: Mid-period in vivo distribution and excretion assessment," Part. Part. Syst. Charact. **1800464**, 1–5 (2018).
12. T. Limongi, M. Canta, L. Racca, A. Ancona, S. Tritta, and V. Cauda, "Improving dispersal of therapeutic nanoparticles in the human body," Nanomedicine **14**, 797–801 (2019).
13. H. Azamal and I. Muhammad, *Nanomaterials and Plant Potential* (Springer, Switzerland, 2019).
14. M. Celentano et al., "Diffusion limited green synthesis of ultra-small gold nanoparticles at room temperature," Colloids Surf., A **558**, 548–557 (2018).
15. A. M. Gamal-Eldeen et al., "Gum arabic-encapsulated gold nanoparticles for a non-invasive photothermal ablation of lung tumor in mice," Biomed. Pharmacother. **89**, 1045–1054 (2017).
16. T. Weil et al., "NIR-emitting and photo-thermal active nanogold as mitochondria-specific probes," Biomater. Sci. **5**, 966–971 (2017).
17. I. Lázár and H. Szabó, "Prevention of the aggregation of nanoparticles during the synthesis of nanogold-containing silica aerogels," Gels **4**, 55 (2018).
18. H. Tsai, P. F. Hsiao, S. Peng, T. Tang, and S. Lin, "Enhancing the in vivo transdermal delivery of gold nanoparticles using poly(ethylene glycol) and its oleylamine conjugate," Int. J. Nanomed. **11**, 1867–1878 (2016).
19. G. Brancolini and V. Tozzini, "Multiscale modeling of proteins interaction with functionalized nanoparticles," Curr. Opin. Colloid Interface Sci. **41**, 66–73 (2019).
20. M. Teimouri et al., "Gold nanoparticles fabrication by plant extracts: Synthesis, characterization, degradation of 4-nitrophenol from industrial wastewater, and insecticidal activity—A review," J. Clean. Prod. **184**, 740–753 (2018).
21. M. Sengani, A. Grumezescu, and V. Rajeswari, "Recent trends and methodologies in gold nanoparticle synthesis—A prospective review on drug delivery aspect," Open Nano **2**, 37–46 (2017).
22. P. Bergese and K. Hamad-Schifferli, *Nanomaterial Interfaces in Biology. Methods and Protocols,* 1st ed., Vol. 1025 of *Methods in Molecular Biology* (Humana Press, Totowa, NJ, 2013).
23. S. T. Kim, K. Saha, C. Kim, and V. M. Rotello, "The role of surface functionality in determining nanoparticle cytotoxicity," Acc. Chem. Res. **46**, 681–691 (2013).
24. R. Handy, F. von der Kammer, J. Lead, M. Hassellöv, R. Owen, and M. Crane, "The ecotoxicology and chemistry of manufactured nanoparticles," Ecotoxicology **17**, 287–314 (2008).
25. D. B. Warheit, "Debunking some misconceptions about nanotoxicology," Nano Lett. **10**, 4777–4782 (2010).
26. L. Packer, E. H. Witt, and H. J. Tritschler, "Alpha-lipoic as a biologycal antioxydant," Free Radic. Biol. Med. **19**, 227–250 (1995).
27. W. Haiss, N. T. K. Thanh, J. Aveyard, and D. G. Fernig, "Determination of size and concentration of gold nanoparticles from UV–Vis spectra," Anal. Chem. **79**, 4215–4221 (2007).
28. B. Varnholt, P. Oulevey, S. Luber, C. Kumara, A. Dass, and T. Bürgi, "Structural information on the Au–S interface of thiolate-protected gold clusters: A Raman spectroscopy study," J. Phys. Chem. C **118**, 9604–9611 (2014).
29. G. Socrates, *Infrared and Raman Characteristics Group Frequencies,* 3rd ed. (Wiley, Hoboken, NJ, 2001).
30. D. Divakaran, J. R. Lakkakula, M. Thakur, M. Kumar, and R. Srivastava, "Dragon fruit extract capped gold nanoparticles: Synthesis and their differential cytotoxicity effect on breast cancer cells," Mater. Lett. **236**, 498–502 (2019).
31. M. Noruzi, D. Zare, K. Khoshnevisan, and D. Davoodi, "Rapid green synthesis of gold nanoparticles using Rosa hybrida petal extract at room temperature," Spectrochim. Acta, Part A **79**, 1461–1465 (2011).
32. S. Enanv, H. Medical, S. Ab, and S. Bertling, Int. Standard **2009** (2009).
33. S. K. Misra et al., "Characterization of carbon nanotube (MWCNT) containing P(3HB)/bioactive glass composites for tissue engineering applications," Acta Biomater. **6**, 735–742 (2010).